analytical chemistry

Perspective

pubs.acs.org/ac

Measurement of Special Nanoparticle Structures by Light Scattering

Philip J. Wyatt*

Wyatt Technology Corporation, Santa Barbara, California 93117, United States

ABSTRACT: The characterization of nanoparticle size and structure by means of classical light scattering measurements from monodisperse suspensions is examined from both the Rayleigh–Gans (R–G) approximation as well as (for various spherical structures) the exact Lorenz–Mie theory. A means by which the traditional limits of the R–G theory may be extended and simplified is shown by a detailed discussion of the characteristic mean-square radius. This becomes particularly important for irregular particle shapes, where scattering depends on the orientation of such particles with respect to the direction of the incident illumination. A variety of particle structures are addressed, including rods, tubes, ellipsoids, rings, and superellipsoids.

With the increasing attention afforded the "nano-world", interest in the unique realm of so-called nanoparticles continues to grow. For the analytical scientist, many of the most important among them are those suspended on liquids, most often aqueous. They appear in many different shapes, sizes, and compositions. Light scattering techniques long have been used to deduce such properties, although some additional *a priori* information may be required. Certain classes of particles are often characterized by a particular model, such as a homogeneous sphere, whose size and average refractive index are often readily derived from the scattering data collected. Generally, the basic objective of comparing light scattering measurements with theory is to extract the particle's structural parameters, most often its size. Thus, by comparing a so-called model with the collected experimental data, a least-squares fitting procedure may be employed to extract the set of structural parameters (such as size) that provides the closest fit. Such a fit is then assumed to represent closely the scattering particle. However, are all of these calculations really needed if, for example, one seeks only the particle's size?

The focus of this perspective is liquid borne particles of various types. Although nanoparticle most commonly refers to particles of size up to 100 nm, the author prefers the more general definition, *viz.*, particles having at least one dimension less than 100 nm. Homogeneous spherical particles represent another special class with sizes up to about 1000 nm. For many such particles, the Rayleigh–Gans (R–G) approximation is sufficient to characterize them well, but as their size becomes comparable to the incident wavelength, severe limitations arise. In addition, the scattering properties of nonspherical particles become difficult to interpret by such approximate theory because their scattering properties vary with their orientation to the incident illuminating beam. Finally, if a distribution of particle sizes is present in any scattering volume, average scattering properties are of little use even for the deduction of their average properties. So, this perspective further focuses on particles of interest that have been effectively fractionated into well-defined monodisperse samples before applying suitable interpretive formulas and techniques. The preferred means for fractionating such particles is discussed as well. Finally, a new approach, starting with some elements of R–G theory, which should permit the measurement of broad classes of particle shapes and sizes with accuracy sufficient for their quantitative characterization, is hypothesized and tested.

PRELIMINARIES AND THE RAYLEIGH–GANS APPROXIMATION

Multiangle light scattering (MALS) measurements have become a far more important tool of the analytical chemist than they were but a few decades ago.[1−3] With the tremendous development, during this same period, of liquid chromatography methods able to separate mixtures of particles based upon their hydrodynamic size, the application of well-understood inverse scattering theories became possible. By such means, many types of molecular and particle ensembles could be measured and classified immediately following separation, and their size distributions could be derived.[4,5] However, interpreting the scattering of monochromatic light from homogeneous spheres, for example, would require application of Lorenz–Mie theory to extract their sizes and distributions. Although such inversions of scattering data to particle structural distributions often required the use of complex scattering theory, within certain limits a relatively simple approximation may be used. Indeed, if scattering particles satisfy certain compositional strictures, the analyses become far simpler. Many of the nanoparticles structures of current interest fall within this restricted range, especially within the fields of protein chemistry, virus like particles, emulsions,

Received: January 15, 2014
Accepted: July 10, 2014
Published: July 21, 2014

   dx.doi.org/10.1021/ac500185w | *Anal. Chem.* 2014, 86, 7171−7183

liposomes, and nanotubes, so a careful examination of the myriad applications of this simplified analysis is presented here.

We begin with a description of the so-called R−G approximation based specifically on the premise that the scattering particles are effectively invisible! By this is meant that the amount of light scattered by the particle because of its presence is vanishingly small and there are effectively no discernible changes to the unscattered incident wave. For this to be valid, there are two requirements

$$\frac{|m^2-1|}{|m^2+2|} \approx \frac{|2(m-1)|}{3} \approx \frac{|m-1|}{3/2} \approx |m-1| \ll 1 \tag{1}$$

where $m = n/n_0$ ($\approx$1), n is the refractive index of the particle, n_0 is the refractive index of the surrounding medium, and

$$x|m-1| \ll 1 \tag{2}$$

where $x = 2\pi a/\lambda$, and $n_0\lambda = \lambda_0$ is the wavelength in vacuum. The particle size is usually defined as equal to $2a$, where, for example, the radius of a spherical particle would be a. Equation 2 is often extended further by recognizing that forward scattered waves do not depart significantly from unscattered waves and, for very small angles, do not depart from the nearly invisible stricture of the R−G approximation, *viz.*

$$2qa|m-1| \ll 1, \quad \text{where } q = \frac{2\pi}{\lambda}\sin\frac{\theta}{2} \tag{3}$$

Thus, even for large particles where eq 2 might fail, by restricting measurement of scattered light to small angles θ, where $2qa|m-1| \ll 1$ and the dimension of the particle is $2a$, the R−G approximation may well provide a means to obtain the particle size from such small angle scattering measurements as long as eqs 1 and 3 are valid. In this R−G approximation, many interesting results may be obtained, especially for applications of liquid chromatography separated samples, which relate to the measurement of size and structure of a variety of important particles, molecules, and their aggregates. For example, the most used and familiar result is that for a homogeneous sphere of radius a. The scattered intensity per unit solid angle per unit incident intensity for incident vertically polarized light of intensity I_0 may be shown as

$$\frac{I}{I_0} = \frac{(ka)^4V^2}{4\pi}|m-1|^2\left[G\left(2x\sin\frac{\theta}{2}\right)\right]^2 = \frac{(ka)^4V^2}{4\pi}|m-1|^2P(\theta) \tag{4}$$

where $V = (4/3)\pi a^3$. The function $G(u)$ is

$$G(u) = \frac{3}{u^3}(\sin u - u\cos u) \tag{5}$$

The function $P(\theta)$ is often referred to as the form factor or particle scattering function. When we review some experiments later, we will see how well this approximation works out as a means to deduce the particle size for homogeneous spheres.

Details of the application of the R−G approximation to other particle structures are given in refs 6 (Chapter 7) and 7. Reference 7 contains explicit expressions for ellipsoids, $(x/a)^2 + (y/b)^2 + (z/c)^2 = 1$, and superellipsoids of revolution given by the equation

$$[|x|/a]^n + [|y|/b]^n = 1 \tag{6}$$

where $n > 2$. As n increases, its shape approaches a smoothly capped cylinder. The bacterial objects considered in ref 7 were all far too large for accurate characterization by the R−G approximation per eq 3, except at extremely small scattering angles. Nevertheless, the examples shown clearly indicate the large number of scattered intensity extrema expected from such objects as well as the clear differences in scattering expected for different shapes and orientations. It is important to emphasize that for any particle whose shape is not spherically symmetric the angular variation of the scattered light will depend upon its orientation with respect to the direction of the incident light. If many such particles are present, each at an arbitrary and random orientation with respect to the direction of the incident illuminating beam, then it is necessary to fit the data to an integrated representation of such random orientations. For certain shapes, this averaging may be expressible in closed form,[6] such as for rods and disks. We shall discuss a simpler approach later.

Using these representations and requiring that the measurements and particles must comply with eqs 1 and 3, the scattered light intensity data measured as a function of angle may be fit to a model assumed appropriate. From such measurements, the associated size parameters, such as length or radius, often may be derived. If the particle structures are not spherical, then this approach will require additional considerations since orientation with respect to the direction of the incident beam may add significant interpretive complications.

Before focusing on applications of the R−G approximation, we should review briefly a related field: the scattering of light by macromolecules in solution. Indeed, the development of the theory required to derive molar masses, among other features, from light scattering measurements is based on the applicability of the R−G theory plus some thermodynamic considerations. In this regard, Debye[8,9] was the first to point out that measurement of the turbidity of a solution combined with knowledge of the number of molecules present per unit volume provided means to determine their molar mass.

The source of the solution turbidity, of course, is the scattering of light passing through it. Referring to eq 4, for example, the removal of light from an incident beam of intensity I_0 passing through a path l is just $I/I_0 = \exp(-l\tau)$, where the turbidity is τ. Following the discussion of Chanda,[10] $\exp(-\tau l) = (I_0 - I_s)/I_0 = (I_0 - I_s'l)/I_0 = 1 - I_s'l/I_0$, where I_s is the total amount of light scattered by the solution and I_s' the amount of light scattered in the passage of the beam through the path l. However

$$\exp(-\tau l) = 1 - \tau l + \frac{1}{2}(\tau l)^2 - \frac{1}{3!}(\tau l)^3 + \cdots \simeq 1 - \tau l \tag{7}$$

Hence, $\tau = I_s'/I_0$. Note that the scattering solute concentration is assumed to be very low, a prerequisite for the development of the theory. The turbidity of the solution may be shown[10,11] to be related to the excess Rayleigh ratio, $R(\theta)$, by

$$\tau = \frac{16\pi}{3}R(\theta) \tag{8}$$

with the final result following Zimm[12] for vertically polarized incident light of wavelength λ_0,

dx.doi.org/10.1021/ac500185w | Anal. Chem. 2014, 86, 7171−7183

$$R(\theta)/(K^*c) = MP(\theta) - 2A_2M^2cP^2(\theta),$$
$$\text{where } K^* = \frac{4\pi^2 n_0^2}{N_A\lambda_0^4}\left(\frac{dn}{dc}\right)^2 \quad (9)$$

In eq 9, N_A is Avogadro's number, M is the weight-average molar mass of the solute molecules at concentration c, n_0 is the refractive index of the solvent, A_2 is the second virial coefficient, and dn/dc is the refractive index increment Δn with respect to the incremental change of concentration Δc. The development of light scattering techniques for the study of dilute solutions of macromolecules, continuing from eq 9, includes a broad range of measurements and research on high molar mass polymers and chains. At extremely dilute concentrations, the second term of eq 9 may be dropped to yield

$$R(\theta)/(K^*c) = MP(\theta) \quad (10)$$

by which both molar mass and size [through $P(\theta)$] may be extracted. As long as the molecules satisfy eqs 1 and 2, their structures could be of any of the types described initially in this perspective by the R−G approximation. The neglect of the fact that application of eqs 9 or 10 also require these same restrictions often results in the application of the R−G approximation in the molecular context when the molecules are far larger than anticipated by the theory. It is here where we must apply eq 3 judiciously by considering more carefully scattering data at very small angles where eq 3 is valid.

THE AVERAGE MASS-WEIGHTED SQUARE OF A PARTICLE'S RADIAL DISTANCE FROM ITS CENTER OF GRAVITY AKA ITS MEAN-SQUARE RADIUS

Let us begin this section with a brief discussion of what we mean by the size of a particle, since this is one of the most important of its features. For a sphere, that is pretty easy: its radius or its diameter. However, other types of particles may not be so easy. Using the sphere as a model, it seems reasonable to provide some sort of radial distance of its mass elements with respect to its center, commonly referred to as its center of mass. (The term center of gravity is often used and may be responsible for the frequently seen subscript g associated with such measure.) From this point, a convenient measure might be the average distance from this center to each mass element of the particle. Thus, every small mass element m_i is at a distance r_i from the center of mass, and a useful measure of the particle's effective size might be something like

$$R_G = \frac{\sum_i m_i r_i}{\sum_i m_i} \quad (11)$$

As it turns out, in the R−G approximation, there is a quantity similar to this that is easily derived from measurements of the light scattered by a monodisperse suspension of such particles/molecules. Rather than yield an average radial distance, the light scattering measurement yields an average square radial distance

$$\langle r_g^2\rangle = \frac{\sum_i m_i r_i^2}{\sum_i m_i} \quad (12)$$

This is the general expression for the mean-square radius, with the g signifying measurement with respect to the center of gravity. So, if we can measure $\langle r_g^2\rangle$ directly, then we may take its square root, $\langle r_g^2\rangle^{1/2}$, and obtain a useful measure of the particle size present. Let us examine the basis for the form factor $P(\theta)$ in more detail beginning with reference to Kratochvil's delightful text.[11]

On the basis, in large measure, of the work of Debye,[8,9] Kratochvil begins with the assumption of a random coil molecule in a fluid that is not affected by external hydrodynamic or electrical forces. Thus, its orientation is randomly changing with respect to the direction of an incident illuminating beam of light. In addition, the molecule is assumed to be composed of small identical mass points i, j, k, ... Assuming that the particle orients itself with equal probability in all directions and is composed of n identical scattering mass points, he (and others, of course) shows that the form factor may be written

$$P(\theta) = \frac{1}{n^2}\sum_{i=1}^{n}\sum_{j=1}^{n}\frac{\sin \mu h_{ij}}{\mu h_{ij}} \quad (13)$$

where h_{ij} is the distance between the ith and jth mass points and $\mu = (4\pi/\lambda)\sin(\theta/2)$. From eq 13, it may be shown that as the scattering angle $\theta \to 0$, $P(\theta) \to 1$. Expanding $\sin \mu h_{ij}$ in a Taylor's series, eq 13 may be written

$$P(\theta) = \frac{1}{n^2}\sum_{i=1}^{n}\sum_{j=1}^{n}\frac{\sin \mu h_{ij}}{\mu h_{ij}} = \frac{1}{n^2}\sum_{i=1}^{n}\sum_{j=1}^{n}\left[1 - \frac{(\mu h_{ij})^2}{3!} + \frac{(\mu h_{ij})^3}{5!} - \ldots\right] \quad (14)$$

However, the product μh_{ij} must be very small, so the form factor $P(\theta)$ may be expressed by its first two terms only, *viz.*

$$P(\theta) \simeq 1 - \frac{\mu^2}{3\cdot 2\cdot n^2}\sum_{i=1}^{n}\sum_{j=1}^{n}(h_{ij})^2 \quad (15)$$

because $\sum_{i=1}^{n}\sum_{j=1}^{n} 1 = n^2$. Following Kratochvil, the summations over all of the squares of the distances, h_{ij}, between the two mass elements may be re-expressed in terms of the squares of the distances of each mass element from the particle's center of mass/gravity with the final result

$$\lim_{\theta\to 0} P(\theta) = 1 - \frac{\mu^2}{3}\langle r_g^2\rangle \quad (16)$$

and $\langle r_g^2\rangle$ as defined in eq 12. Here, a mass element m_i lies at a distance r_i from the coil's center of gravity (mass). In Kratochvil's analysis above and most others, the individual mass elements m_i are assumed identical, i.e., throughout the molecule each mass element i occupies the same volume at location i. The concept of a mean-square radius was described earlier, for example, by Zimm[12] for a linear coiling chain molecule of uniform degree of polymerization n and average link size b. For such a molecule, the average end-to-end distance squared, $h^2 = b^2n$, with its associated mean-square radius $\langle r_g^2\rangle = h^2/6$. Equation 16 becomes

$$\lim_{\theta\to 0} P(\theta) = 1 - (8\pi^2/9\lambda^2)h^2\sin^2\frac{\theta}{2} \quad (17)$$

On this basis, it may be shown that any molecule or particle may be represented (in the R−G approximation) as being composed of small mass elements m_i located, respectively, at a distance r_i from its center of gravity. Thus, by measuring the initial variation of scattered light (slope, i.e, $dP(\theta)/d[\sin^2\theta/2]$) at very small scattering angles, we may determine the particle's

dx.doi.org/10.1021/ac500185w | Anal. Chem. 2014, 86, 7171−7183

mean-square radius directly and independent of any *a priori* knowledge of the particle's shape or orientation. If the particle is of homogeneous density, ρ, then eq 12 becomes simply

$$\langle r_g^2 \rangle = \frac{\sum m_i r_i^2}{M} = \frac{\sum v_i r_i^2}{V} = \frac{1}{V} \iiint R^2(r,\theta,\varphi)\, \mathrm{d}v \qquad (18)$$

where the total particle volume is V, $M = \rho V$, $m_i = \rho v_i$, and R is the distance from the center of mass of M to the volume element dv.

Equation 16, relating the slope of $P(\theta)$ with $\sin^2 \theta/2$ at $\theta = 0$ to the particle/molecule mean-square radius, seems to have been presented initially by Zimm and other colleagues from their investigations of the extraction of molar mass from light scattering measurements. This relation was discussed explicitly by Kerker[13] in his chapter on R−G scattering, but he never seems to have taken it further. This author has never seen this relationship explicitly discussed in any of the literature[6] describing/discussing the R−G approximation except during concurrent discussions relating to measurements of molar masses and their interactions. Interestingly, Kerker's earlier paper[14] with Farone and Matijevic focused on the applicability of the R−G approximation to represent the exact Lorenz−Mie theory[15−18] that describes the scattering by a homogeneous sphere. Their paper compared differences between the total scattering cross-section as well as specific scattered intensities at 10, 20, and 45°. To what end? Eventually the hope was to interpret scattering measurements in order to derive particle size. Be that as it may, it remains surprising that so much effort (including that of the author) has gone into the fitting of scattering data directly to a particular R−G particle shape function (e.g., tumbling rods and disks per ref 6) in order to derive particle size. This should be compared to a determination of the rms radius from measurement of the initial slope (at $\sin^2 \theta/2 = 0$) of $P(\theta)$, from which a very good measure of size may be derived with negligible effort.

Before leaving this section, it should be emphasized that the R−G approximation assumes that the mass elements m_i of the total particle mass M are each considered independent Rayleigh scatterers. Thus, the scattering by such a particle is assumed entirely due to the scattering of the independent, non-interacting, particle elements. The only effect they have upon the variation of the scattered intensity with scattering angles θ and φ is their relative excitation in phase with the incident wave. Thus, particles, in the R−G approximation, are assumed to be composed of (generally) rigidly attached Rayleigh scatterers. More traditional particles such as, for example, polystyrene latex spheres, scatter in a manner more complex than the mere in-phase R−G constituents that might have been assumed to be the basis of their interaction with an incident plane wave. For such structures, the incident wave may induce other fields within the illuminated particle producing scattered radiation that would be of a polarization different than the illuminating source. All light scattered by a R−G particle, since all of its constituents are independent Rayleigh particles much smaller than the incident wavelength, is of the same polarization as the incident light, i.e., in all scattering planes, the scattered light is of the same polarization as the incident light. Sometimes, however, the scattering by particles that are not R−G scatterers is, nevertheless, well characterized by some of the assumptions and characteristics of an R−G structure. We shall return to these particles later in this perspective. At this time, however, we should not lose sight of the continuing importance of the mean-square radius and its possible extension well beyond the limits of the R−G approximation itself.

THE MEAN-SQUARE RADIUS AND ITS RELATION TO PARTICLE SHAPE

In an early paper by Debye[9] on the determination of molar mass from light scattering, he proposed that by determining the coefficients α_n of the expansion of $P(\theta) = 1 - \alpha_1 \sin^2(\theta/2) + \alpha_2 \sin^4(\theta/2) - \ldots$ [a generalization of eq 16] the shape of a particle might be obtained from an experiment wherein the variation with angle of the scattered intensity is measured. Kratochvil, however, emphasizes that attempting to determine the shape of a particle by trying to fit its scattering function to that expected from a particular model has many problems associated with the procedure. Although his conclusions were generally directed to high molar mass polymers, his observations and suggestions have relevance also to particles (as specified by Debye[9]). Among these, he includes the need to make measurements from monodisperse samples because polydisperse scatterers would significantly diminish the shape-dependent data. The need to fractionate particles, in any event, before measurement cannot be over emphasized. Kratochvil stresses also the need to make such measurements over as broad a range of scattering angles as possible (MALS) in order to see features characteristic of different sizes and shapes. In this regard, it is important to pay close attention to eq 3, as it affects the results derived from eq 16. Once that relation no longer holds, the deductions based on the R−G approximation lose their significance. Indeed, as we soon shall see, it is necessary to restrict the range of scattering angles used for the application of eq 16.

As mentioned in the first section of this perspective, in the R−G approximation, there are some closed-form expressions for the form factor $P(\theta)$, such as eq 4 that describes homogeneous spheres, *viz.*, $P(\theta) = [G(u)]^2$. For long, infinitely thin rods of length L averaged over their random orientations with respect to the incident illumination, we have

$$P(\theta) = \frac{1}{z} \int_0^{2x} \frac{\sin w}{w}\, \mathrm{d}w - \left(\frac{\sin z}{z}\right)^2 \qquad (19)$$

where $z = kL \sin(1/2)\theta$.

The mean-square radius of a random coil, $h^2/6$, was one of the first derived.[9,11,19] For such random coils, we have

$$P(\theta) = (2/u^2)[\exp(-u) - 1 + u] \qquad (20)$$

where $u = (8\pi^2 h^2/3\lambda^2) \sin^2 \theta/2$, and the mean-square end-to-end distance of the coil, $h^2 = nb^2$. A closed form for a sphere with a concentric shell of refractive index different from that of its core may be found in ref 20, and an expression for randomly oriented thin disks of radius a, in ref 6.

Rather than trying to deduce the shape and size of a particle from the collected scattering data (a variant of the so-called inverse scattering problem[21]), it is important to have available an *a priori* knowledge of the particle shape. Such information often may be obtained from measurements of the sample by electron or atomic force microscopy. From there, the sizes associated with the assumed shape may be derived from the mean-square radii, an automatic and important consequence of the R−G approximation. Thus, by knowing that a suspension is composed, for example, of very thin rods, deriving the mean square radii for a separated size fraction will permit deduction of the length (and perhaps the diameter, if some additional data

dx.doi.org/10.1021/ac500185w | *Anal. Chem.* 2014, 86, 7171−7183

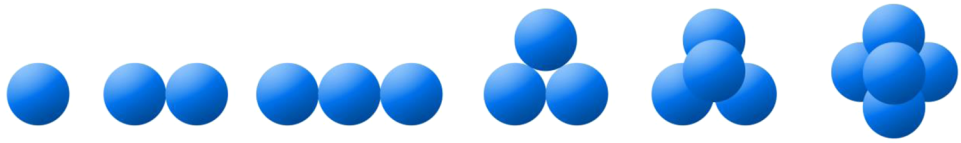

$\langle r_g^2 \rangle$	$(3/5)a^2$	$(8/5)a^2$	$(49/15)a^2$	$(29/15)a^2$	$(92/45)a^2$	$(29/15)a^2$
	$0.6a^2$	$1.6a^2$	$3.267a^2$	$1.93a^2$	$2.04a^2$	$1.93a^2$
$\langle r_g^2 \rangle^{1/2}$	$0.77a$	$1.265a$	$1.807a$	$1.39a$	$1.43a$	$1.39a$

Figure 1. Mean-square radii for aggregates of 2−5 homogeneous spheres.

are available) of rods separated in that fraction. This does not mean, however, that for spherically symmetric particles (the only forms where scattering is not dependent on orientation with respect to the direction of the incident illumination) such a fitting process cannot be used. We shall explore some such examples later.

Let us calculate the mean-square radii of some additional structures. We begin with a homogeneous sphere of radius a and density ρ. Its center of gravity (mass), of course, is at its center, and its volume is $(4/3)\pi a^3$, so eq 18 becomes

$$\frac{4}{3}\pi a^3 \langle r_g^2 \rangle = \iiint R^2(r,\theta,\varphi)\, \mathrm{d}v = \int_0^{2\pi} \mathrm{d}\varphi \int_0^{\pi} \sin\theta\, \mathrm{d}\theta \int_0^a r^4\, \mathrm{d}r = \frac{4\pi}{5}a^5 \tag{21}$$

Therefore, $\langle r_g^2 \rangle = (3/5)a^2$.

Consider, next, an aggregate of two spheres each of radius a. The complex scattering by such a structure has been considered[22] in detail and for cases, as well, when the two spheres do not touch. The center of mass of the aggregate lies at their point of contact, a distance a from each of their individual centers of mass. We must integrate the square of the distance from this point with respect to each volume element of the two spheres. Such volume elements lie at a distance ρ from the center of mass of the two-sphere assembly, where $\rho^2 = (r \sin\theta)^2 + (a - r\cos\theta)^2$. Thus

$$\begin{aligned} V\langle r_g^2 \rangle &= 2\int_0^{2\pi} \mathrm{d}\varphi \int_0^{\pi} \sin\theta\, \mathrm{d}\theta \int_0^a \rho^2 r^2\, \mathrm{d}r \\ &= 2\left[\int_0^{2\pi} \mathrm{d}\varphi \int_0^{\pi} \sin\theta\, \mathrm{d}\theta \int_0^a r^2(a - r\cos\theta)^2\, \mathrm{d}r\right] \\ &= 2\left[\int_0^{2\pi} d\varphi \int_0^{\pi} \sin\theta\, \mathrm{d}\theta \int_0^a r^2(r^2 + a^2)\, \mathrm{d}r\right] \end{aligned} \tag{22}$$

because $\int_0^{\pi} \cos\theta \sin\theta\, \mathrm{d}\theta = 0$. Finally, with the volume of the 2 spheres $V = 2((4/3)\pi a^3)$, we have

$$\begin{aligned} \langle r_g^2 \rangle &= 2\left[\int_0^{2\pi} \mathrm{d}\varphi \int_0^{\pi} \sin\theta\, \mathrm{d}\theta \int_0^a r^4\, \mathrm{d}r + a^2\right]/V \\ &= 2\left[\frac{4}{5}\pi a^5 + a^2\frac{4}{3}\pi a^3\right]/2\left(\frac{4}{3}\pi a^3\right) = \frac{3}{5}a^2 + a^2 = \frac{8}{5}a^2 \end{aligned} \tag{23}$$

A set of additional equal-sphere aggregates and their corresponding mean-square radii are shown in Figure 1. Note the identical results for the five- and three-sphere aggregates (not the linear three-sphere structure). Because the center of mass of each sphere is at exactly the same distance from the center of mass of the three and five element aggregates, the mean-square average is the same for both arrangements. The addition of scattering elements generally does not produce an increase in the average distance of all of the elements present from the aggregate center of mass. Because MALS measurements are used to derive such mean-square radius values, how can different structures, such as the three- and five-sphere aggregates be differentiated? Because the three-unit sphere aggregate will have only $^3/_5$ the molar mass of that of the five-unit aggregate, the differentiation, of course, might require measurement of the aggregate molar mass if the particles can be considered to lie within that molecular realm per eqs 9 or 10. However, here we would be leaving the particle regime and returning to solvated molecular structures. In any event, focusing entirely on particles, we would expect their effective hydrodynamic sizes to be different and thus differentiable following a variety of separation techniques.

Let us next consider additional structures. A tube of length L, thickness t, and radius a; a homogeneous rod of length L and radius a; a plank of length L, thickness t, and width w; and an ellipsoid of revolution semiminor and semimajor axes a and b, respectively. For the more general ellipsoid, the semiaxes are a, b, and c. Finally, a ring of outer radius a and square cross-section thickness t. It is not difficult to show from these examples that their corresponding mean-square radii are given by

$$\text{tube} \quad \langle r_g^2 \rangle = \frac{L^2}{12} + a^2 + \frac{t^2}{2} - at \tag{24}$$

$$\text{rod} \quad \langle r_g^2 \rangle = \frac{L^2}{12} + \frac{a^2}{2} \tag{25}$$

$$\text{disk} \quad \langle r_g^2 \rangle = \frac{a^2}{2} + \frac{t^2}{12} \text{ (radius } a \text{ and thickness } t\text{)} \tag{26}$$

$$\text{plank} \quad \langle r_g^2 \rangle = \frac{1}{12}(L^2 + t^2 + w^2) \tag{27}$$

$$\text{ellipsoid of revolution} \quad \langle r_g^2 \rangle = \frac{2a^2 + b^2}{5} \tag{28}$$

$$\text{ellipsoid} \quad \langle r_g^2 \rangle = \frac{a^2 + b^2 + c^2}{5} \tag{29}$$

$$\text{ring} \quad \langle r_g^2 \rangle = a^2 - at + \frac{7}{12}t^2 \tag{30}$$

Other important structures include hollow spheres of radius a and thickness t and two-sphere aggregates with spheres of different radii $a > b$.

dx.doi.org/10.1021/ac500185w | Anal. Chem. 2014, 86, 7171−7183

hollow sphere, radius a and thickness t

$$\langle r_g^2 \rangle = \frac{3}{5}a^2\frac{[1-(1-x)^5]}{[1-(1-x)^3]},\ x = \frac{t}{a} \tag{31}$$

spherical shell $\langle r_g^2 \rangle = a^2$ (32)

two spheres, $a > b$

$$\langle r_g^2 \rangle = \frac{3}{5}\frac{(a^5+b^5)}{(a^3+b^3)} + \frac{a^3(a-x)^2 + b^3(b+x)^2}{(a^3+b^3)},$$
$$x = \frac{a^4-b^4}{(a^3+b^3)} \tag{33}$$

Note that eq 31 yields the result, eq 32, as $t \to 0$. From eq 33, when $b = a$, we have the result of eq 23, *viz.*, $(8/5)a^2$.

THE RIGHT TYPE OF EXPERIMENT

Following Kratochvil's emphasis of the need for monodisperse samples, polydisperse samples must be fractionated in order to avoid analytical complications associated with unraveling the mass and size distributions present in a sample. With the advent of means to separate molecules and particles by liquid chromatography techniques including size-exclusion chromatography (SEC), field-flow fractionation (FFF), reversed-phase chromatography, and their many variations, it has become standard practice to separate samples first by these methods and then measure the effectively uniform fractions within an eluting slice by means of differential refractive index (dRI) refractometers, UV absorption, multiangle light scattering (MALS), and/or dynamic light scattering. For the present perspective, whose techniques, we hope, will yield the distributions of various structural features present, we will be focusing most attention on features disclosed from MALS following separation.

Although SEC processes[23] have long been the separation method of choice for both molecules and particles, in recent years separations based on FFF[24] have become the overwhelming choice for particles, with particular focus on asymmetric flow FFF (A4F). One of the traditional problems of SEC has been the shedding of column packing materials (causing superfluous scattered light) in addition to their directly interacting with the analyte itself. Many types of samples, especially proteinaceous particles and materials, often adhere to and sometimes interact with the column constituents. With A4F, on the other hand, interactions with the associated channel structure are negligible. Other SEC problems include, depending upon column packing and flow rates, shear processes that affect the particles sizes derived. Fragile particles such as emulsions and liposomes are not suitable for separation by an SEC column. The relatively gentle fluid separations achieved by A4F channels often provide separations of such particles with negligible effects on their size distributions. It has taken many years for this realization to take hold. First emphasized by the author in his earlier paper[25] on submicrometer particle (nanoparticle) measurement by MALS following FFF separation, the method has become the standard procedure.

Separation in A4F channels is based on the particle/molecule hydrodynamic radius. For the sphere aggregates discussed earlier, their separation on such basis, irrespective of their rms radii, is effective because their hydrodynamic radii are different.

The measurement, therefore, of particles well-characterized by the R−G approximation is best achieved by light scattering measurement of monodisperse samples; the latter being produced by A4F separation, athough, often, fractionation techniques may suffice also. At the sufficiently low concentrations required of molecules so that eq 10 is valid, the measurement of such solvated molecular concentration is not needed unless their molar mass must be determined as well. Indeed, whereas a differential refractometer or UV detector is required following the MALS instrumentation for the determination of concentration and, thereby molar mass, for many types of particles, their absolute differential number distributions may be determined immediately[25,26] without such detectors. It is important to note for this particle−molecule dichotomy that the smallest particle measurable by MALS is approximately $\lambda/30$. For a spherical particle, this corresponds to about a 10 nm radius.

INSTRUMENTATION AND SOFTWARE

All measurements presented and discussed in this perspective were fractionated using the Eclipse A4F system in series with the HELEOS MALS instruments and the T-rEX differential refractometer, all by Wyatt Technology Corporation (Santa Barbara, CA). The scattering angles, θ, at which aqueous-based measurements were made for the experiments presented here, are shown in Table 1. Note that the scattering angles measured are slightly different for the two types of glass cells commonly used: fused silica and K5. Polystyrene latex (PSL) spheres were measured at $\lambda = 658$ nm in fused silica cells, whereas cellulose rods and carbon nanotubes were measured in K5 scattering cells. Also shown in this table are the corresponding values of $\sin^2 \theta/2$ for particular reference to eq 16.

Table 1. Light Scattering Detector Angles, θ, and $\sin^2 \theta/2$

detector	scattering angle (fused silica)	$\sin^2 \theta/2$	scattering angle (K5)	$\sin^2 \theta/2$
1	na		na	
2	13.0°	1.28×10^{-2}	na	
3	20.7°	3.23×10^{-2}	14.4°	1.59×10^{-2}
4	29.6°	6.53×10^{-2}	25.9°	5.02×10^{-2}
5	37.5°	1.03×10^{-1}	34.8°	8.94×10^{-2}
6	44.8°	1.45×10^{-1}	42.8°	1.33×10^{-1}
7	53.1°	2.00×10^{-1}	51.5°	1.88×10^{-1}
8	61.1°	2.58×10^{-1}	60.0°	2.50×10^{-1}
9	70.1°	3.30×10^{-1}	69.3°	3.23×10^{-1}
10	80.1°	4.14×10^{-1}	79.7°	4.11×10^{-1}
11	90.0°	5.00×10^{-1}	90.0°	5.00×10^{-1}
12	used for DLS		100.3°	5.89×10^{-1}
13	109.9°	6.70×10^{-1}	used for DLS	
14	120.1°	7.51×10^{-1}	121.2°	7.59×10^{-1}
15	130.4°	8.24×10^{-1}	132.2°	8.36×10^{-1}
16	140.0°	8.83×10^{-1}	142.5°	8.97×10^{-1}
17	149.0°	9.29×10^{-1}	152.5°	9.44×10^{-1}
18	157.7°	9.63×10^{-1}	163.3°	9.79×10^{-1}

The analyses of the collected MALS data were all performed by the associated ASTRA (version 5.0 or 6.0) software. Although developed primarily for the interpretation of MALS measurements of polymer and protein solutions, it has been expanded significantly in the past decade to include a variety of calculations, including the application of the R−G approximation to a variety of both molecular and particulate shapes

dx.doi.org/10.1021/ac500185w | Anal. Chem. 2014, 86, 7171−7183

and structures. It is this application that permits, for a variety of shapes and sizes, the direct calculation of the mean-square radius of many types of structures falling within the R−G strictures discussed earlier. In addition, it contains analytical tools capable of analyzing homogeneous spherical molecules/particles based on the Lorenz−Mie[15−18] solution of Maxwell's equations. Data collected during such measurements incorporate the experimentally derived standard deviations associated with the basic MALS measurements themselves. The software includes extensive capabilities for the measurement and analyses of a variety of molecular and particulate samples by quasi elastic light scattering [aka dynamic light scattering (DLS)]. They are not included here.

EXPERIMENTAL OBJECTIVES

The types of particles to be considered in the examples that follow (spheres and rod-like structures) all have an associated form factor, $P(\theta)$, corresponding to an average over all the possible orientations with respect to the direction of the incident beam. For rod-like structures (including tubes) whose diameters are negligible compared to their lengths, the $P(\theta)$'s have the form of eq 19. The objective of the measurements that follow is to demonstrate the means by which MALS data collected from the fractionated particles may be used to derive their size. For spheres, of course, this implies measurement of their radii and, eventually, means to determine their radius and number distributions. For rod-like structures, we hope to measure their lengths and their corresponding distributions. However, for more complicated structures such as the spherical aggregates of Figure 1, ellipsoids, tubes, and superellipsoids, there are no extant forms in the R−G approximation corresponding to the averaging process incorporated into eq 19. Reference 7 addresses this averaging numerically for an ellipsoidal structure characteristic of the shape of typical *Escherichia coli* bacteria, since there is no closed form of $P(\theta)$ averaged over all possible ellipsoid orientations. However, this is an extremely time-consuming and complex task for all but the simplest of structures. So, how can such dimensions be derived, even in the R−G approximation? The solution, of course, is to use the derived root-mean-square radius; a tool that the author believes is all too rarely applied.

The difficulty with the use of the rms radius arises from its definition, i.e., the measured slope (at $\sin^2 \theta/2 = 0$) of the form factor $P(\theta)$. Subject, as well, to eqs 2 or 3, experimental errors of such small angle measurements will affect the precision of the so-derived results. Nevertheless, over a surprisingly broad range of sizes and structures, the errors of sizes derived from experimentally measured rms radii are generally less than 10%. So, whereas Kerker[13,14] and his colleagues sought to find regimes wherein the angular variation (for spheres only) of the R−G approximation agreed well with the exact Lorenz−Mie theory, the far more important size itself will be shown to be readily extracted from the derived rms radii. In order to estimate the accuracy of the results thus obtained, the results for homogeneous spheres will be compared with the Lorenz−Mie theory as well as the R−G approximation of eq 5. For rods and tubes, the results based on derivation of length from the rms radii measured for rods will be compared to the thin tumbling rod approximation of eq 19.

An additional question that should be addressed is how large a particle may be characterized from such measurements in view of the R−G restrictions of eqs 2 and 3? As mentioned above, the Lorenz−Mie formalism, whose characterization of homogeneous spheres has no restrictions (i.e., is not an approximation), should help to provide a good measure for such size limitations. Because the intensity of a wave scattered by a sphere exhibits a series of extrema whose numbers increase with its size, in order to extract its size from such measurements, one needs a sufficient set of scattering data over a broad range of scattering angles. If the MALS system has a finite number of detectors (often arranged somewhat uniformly in $x = \sin \theta/2$), the number of detectors needed to span and to be able to fit such data is on the order of $2ka$, where $k = 2\pi n_0/\lambda_0$. For a sphere of radius 500 nm in water and an incident wavelength of 658 nm, this number is about 13. Note that even with particles this large, if eq 1 is valid, then one should be able to extract such a size, even in the R−G approximation, by calculating slopes at very small angles and using eq 16 so that eq 3 applies. We will look at this concept soon in more detail.

The experimental data presented are intended for illustrative purposes only, and some details of the experimental measurements have been omitted.

HOMOGENEOUS SPHERES

The precision of MALS measurements following a traditional (two separate pumps producing transverse flow and channel flow, respectively) cross-flow FFF separation was clearly demonstrated in the analysis[28] of an extraordinary NIST 100 nm polystyrene latex (PSL) standard (NIST 1963) produced at the then National Bureau of Standards in 1963. The measurement provided an average radius of 50.0 nm with a fwhm (full width at half-maximum) of 0.5 nm! No standard of such narrow distribution has ever been produced since. The MALS data from the standard was contrasted to a 100 nm broad sample (3100-01, produced by Duke Scientific). The size of each eluting fraction was determined by fitting the MALS data as a function of angle to the Lorenz−Mie solution. Each included angle datum was weighted by its reciprocal standard deviation. The separations for that early experiment were made using a traditional cross-flow FFF fractionator in contrast to the A4F devices, now adopted universally. There was no attempt either to simplify the measurement process by trying to interpret the results using the R−G (sphere) approximation or to determine size based on extracting the mean-square radii of the separated PSL particles. These latter simplifications are a major objective of this perspective.

In 2012, an original NBS 1963 PSL vial was recovered and provided the opportunity to repeat the measurement of Wyatt and Villalpando[28] using an A4F channel (single pump) and the newest MALS system available (HELEOS II MALS). The results of these measurements yielded an average particle radius of 50 nm and a fwhm of 0.4 nm! The derived rms radius of 39.0 ± 0.1 nm for each slice per eq 21 yielded an almost perfect result, i.e., $[(5/3)\langle r_g^2\rangle]^{1/2} \approx 50.31 \pm 0.13$.

In order to examine further the ability of the ASTRA software to measure particles, some recent PSL data (unpublished) by Dr. Wei Gao of the Dow Chemical Company (formerly with a division of Rohm and Haas purchased by Dow) have been studied and interpreted here. For one of the finest tests performed to date to confirm the A4F separation efficiency, she prepared a mixture of different PSL samples and then separated them using an Eclipse A4F system. They included particles of nominal diameters of 97 ± 3, 200 ± 6, 296 ± 6, 498 ± 9, and 994 ± 21 nm. The analyses of these and other types of particulates in the present perspective have been

dx.doi.org/10.1021/ac500185w | *Anal. Chem.* 2014, 86, 7171−7183

used to establish some limits of the measurement and interpretive processes to characterize even large particles. These measurements were made at a wavelength of 658 nm. Figure 2 shows the 90° MALS signal at each collection slice

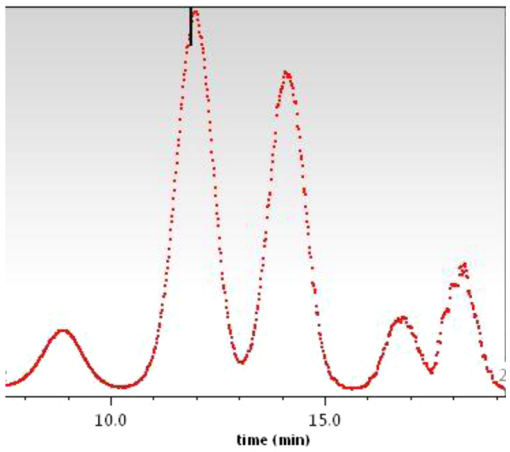

Figure 2. 90° scattering from fractionated mixed PSL sample.

following A4F separation of the mixed sample. Each collected fraction provides a corresponding measure of the scattered light intensity at each detector. The dark vertical line near the top of the second peak in the shaded area corresponds to slice 717 with its associated scattering data shown in Figure 3. This peak

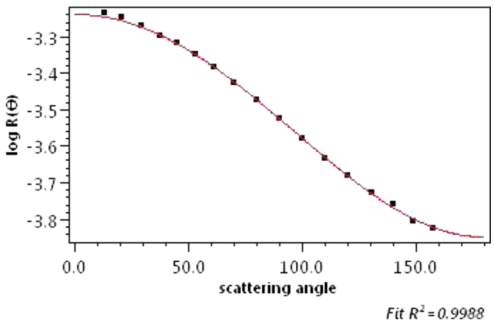

Figure 3. Slice 717 of the 200 nm PSL sample of Figure 2.

corresponds to the fractionated PSL spheres of nominal 200 nm diameter. With a corresponding refractive index of about 1.59, eq 1 yields $|m - 1| = |(1.59/1.33) - 1| = 0.195$, a value <1.0 but certainly not ≪1.0. The value of $x = 2\pi a/\lambda = 1.27$ for $a = 100$ nm. Thus, the restriction of eq 2 is not well satisfied either because it yields $0.195 \times 1.27 = 0.25$, which is certainly not ≪1. Nevertheless, $x|m - 1| < 1$ still produces good quantitative results, with the R−G approximation of eq 4 yielding 98.9 ± 0.2 compared with the Lorenz−Mie exact result of 96.8 ± 0.2. The rms radius, based on the initial slope, produces values of 80.9 ± 8.1, corresponding to radii of 104 ± 10. All three results are in agreement.

Once the radius reaches 500 nm, $x = 6.37$ and eq 2 yields 1.24. This would certainly suggest that trying to fit a R−G approximation, based on eqs 4 and 5, might be a poor choice. Slice 1116 corresponds to a Lorenz−Mie radius of 499 ± 6, the R−G sphere model of eq 4 yields 532 ± 20, and the rms radius of 388 ± 15 corresponds to 500 ± 19. As particles become large, the significance of size results based on the R−G approximation and the derived rms radii suggests this same type of approximation may well be applicable for particles of diameters of the order of 1 μm even though they are not spheres.

For so simple an object as a homogeneous sphere, then what is the limit for MALS measurements to yield a reasonable value? These particles are certainly not true R−G particles, yet the theory and especially use of the rms radius calculation to obtain reasonable size parameters suggests the utility of such an R−G derived value for their characterization. Let us examine the data derived from the measurements presented in Figure 2 from three distinct perspectives:

(a) The Lorenz−Mie theory (an exact solution provided sufficient angular data are available);
(b) The sphere model R−G approximation of eqs 4 and 5, where $P(\theta) = (9/u^6)(\sin u - u \cos u)^2$;
(c) Measurement of the root-mean-square radius, $\langle r_g^2 \rangle^{1/2} = (3/5)a^{1/2}$, whereby the sphere radius $a = (5/3)^{1/2}\langle r_g^2 \rangle^{1/2} \simeq 1.29\langle r_g^2 \rangle^{1/2}$.

Perspectives (b) and (c), of course, are based on the R−G approximation. For perspective (c), eq 3 might provide an answer if the mean-square radius could be derived subject to the further requirement of eq 16, i.e., measurement of the slope at the origin. Yet, the particles, as mentioned, may well be close enough. In terms of the selected 685 slices between the two vertical bars, each collected value corresponds to a slice label between 462 and 1147. The 50, 100, 150, 250, and 500 nm nominal radii lie, correspondingly, within the slice ranges from 462 to 622, 622 to 785, 785 to 938, 938 to 1051, and 1051 to 1147. Note that none are baseline-separated, with some peaks showing significant overlap, corresponding to inadequate separation, between 100 and 150 nm and between 250 and 500 nm. In regions where significant mixtures of two sizes are present, a model based on a single size will not provide an adequate representation of the two populations present. Again, as Kratochvil implied, when only a single species is present, will MALS measurements yield reliable size information.

In Table 2, a few slices from each separated population near its peak (to avoid, as much as possible, the presence of particles

Table 2. Selected Slices from the Elutions Shown in Figure 2[a]

slice	radius L−M	radius sphere model	rms radius	radius
519	48.6	49.5	32 ± 9	42 ± 11
529	49.1	49.8	33 ± 7	42 ± 9
539	49.2	50	31 ± 6	40 ± 8
716	96.7	98.9	73.0 ± 4	94 ± 5
720	96.3	98.3	75 ± 4	97 ± 5
724	97	99	73 ± 4	94 ± 5
838	144.5	155	124 ± 10	160 ± 13
848	144.5	155	123 ± 10	159 ± 13
858	145	155	122 ± 9	158 ± 12
995	246	270	203 ± 6	262 ± 8
1000	246	270	206 ± 6	266 ± 8
1005	246	270	205 ± 6	265 ± 8
1104	491 ± 10	516 ± 25	386 ± 15	498 ± 19
1109	498 ± 8	528 ± 21	388 ± 15	501 ± 19
1121	505 ± 6	541 ± 18	389 ± 19	502 ± 25

[a]Each corresponding radius is based on the Lorenz−Mie theory (column 2) and the sphere model of the R−G approximation (column 3). The R−G approximation-based rms radius $\langle r_g^2 \rangle^{1/2}$ is listed in column 4, and the radius derived therefrom is listed in column 5.

dx.doi.org/10.1021/ac500185w | Anal. Chem. 2014, 86, 7171−7183

from adjacent peaks/species) are listed together with their associated radii as derived from the exact Lorenz−Mie theory (a), the sphere model of (b) above, and the root-mean square (rms) radius with its associated particle radius derived per (c). In order to derive the initial slope to make use, thereby, of the rms radii, all of the data collected are fit with a simple polynomial of order 5 to 10, depending on the anticipated size range being measured. The resultant scattering curve will not, in general, be specific to a particular model; however, its slope at the origin will determine its mean-square radius, provided that the strictures of the R−G theory of eq 3 are valid.

The key to deriving accurate rms radii is measuring the initial slope, and that, in turn, requires very accurate small angle data where eq 16 is valid. For some of the data presented here, these expectations were not well fulfilled. A few comments should be made regarding the quality of each datum. Some small angle data (at 13 and 20.7°), as measured at some slices, are too noisy and need to be dropped from the subsequent (*a*, *b*, or *c*) fitting method. Most slice measurements, however, provide usable data at all 14 angles. On occasion, the exact Lorenz−Mie formalism may collapse with no fit attainable unless certain small angle data are dropped. The R−G sphere approximation fit had similar problems. For the most part, the rms radii data (*c*) produced a reasonable result, i.e., within about 10% of the correct Lorenz−Mie result. Note the extraordinarily large standard deviations frequently seen at the largest sizes considered (diameter 1000 nm). In terms of speed and results, however, method *c* was by far the simplest. The fact that simple particles as large as 1000 nm produce data readily converted into a meaningful sizes is encouraging, especially in the context of using the rms radii. We may conclude, therefore, that if we have some *a priori* knowledge of the particle shape (e.g., obtained by AFM) and that such particles satisfy eqs 1 and 3, deduction of the rms radii alone appears to allow deduction of the particle's associated size. We shall explore such a conclusion presently for the case of nanorods and tubes and discuss its basic simplicity further.

RODS AND TUBES

Cellulose Rods. Figure 4 shows the elution profile (90° scattering) of a cellulose sample[27] composed of very thin rods/

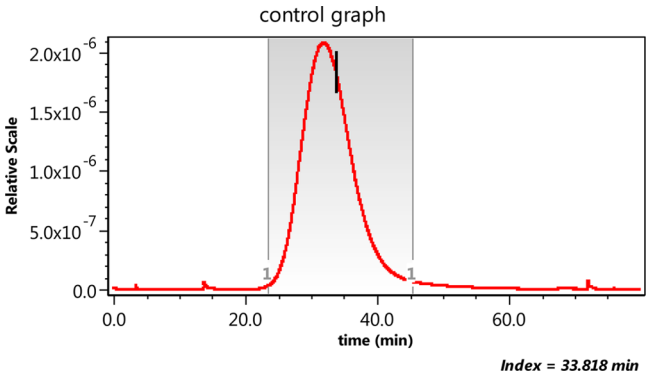

Figure 4. 90° scattering from cellulose rods.

planks. Their effective diameters were much smaller than their lengths. Accordingly, each of eqs 24, 25, and 27, corresponding to tube, rod, and plank, respectively, reduce simply to $\langle r_g^2 \rangle = L^2/12$, the usual result for the vanishingly thin rod model. The refractive index of cellulose[29] at 658 nm is 1.47, so eq 1 yields $|m - 1| = |(1.47/1.33) - 1| = 0.105 < 1$. Figure 5 presents the rod length at each eluting slice based on the rod model. It is

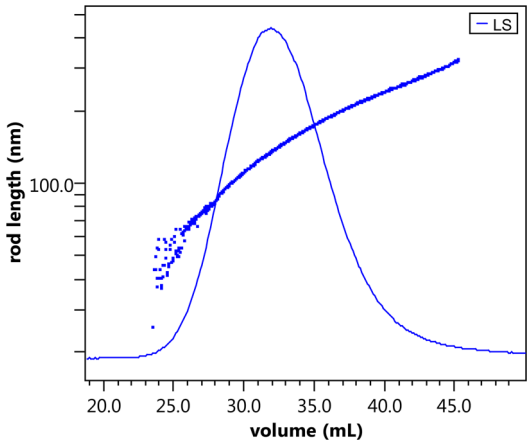

Figure 5. Cellulose rod length as a function of elution volume.

superimposed over the elution curve of Figure 4. Determining the rod length using the measured mean-square radius is certainly simpler than applying eq 19, but the results are comparable. Once we consider higher refractive index rods such as carbon nanotubes (discussed below), the rod model begins to fail significantly in fitting the data.

A most important and far more extensive study of such cellulose-like particles was performed by the LSU group in the paper by Guan et al.[30] Although focused primarily on interpretations based on the simple R−G approximation rod model convoluted with somewhat irrelevant molecular mass considerations, the wealth of data presented provides an invaluable insight into these remarkable particles. The data presented, especially comparisons between TEM measurements and A4F-MALS, represent a significant confirmation of the MALS methodology. The importance of ancillary measurements such as by TEM is well-presented. In this regard, the paper also provides significant support for the application of more complex models to characterize the fractions processed. (see More General Shapes and the rms Radius Revisited, below.)

Carbon Nanotubes. Studies of carbon nanotubes have become very important in recent years, with a great many of them using MALS and other light scattering techniques for their characterization. Their discovery and properties are described in a review article by Ando.[31] Of particular interest for this perspective were measurements[32,33] of so-called single-wall carbon nanotubes (SWCNT), often separated[34,35] by A4F techniques[24] discussed earlier. Some of the interpretations of refs 34 and 35 are confusing in some respects. The measurements reported are, in many instances, exceptional. Yet, the papers focus often on procedures commonly used to extract molar masses and sizes based on the graphical manipulations associated with so-called Zimm, Berry, or Debye plots, rather than the R−G approximation associated with particle size and structure. If the objective of an experimental measurement is the determination of the size and structure of particles in suspension, then molar mass properties are irrelevant. One should not forget that molar mass determinations require concentration detectors as well as d*n*/d*c* values. For particle measurements, these are extraneous. Certainly the molar mass of very small particle-like objects is

dx.doi.org/10.1021/ac500185w | *Anal. Chem.* 2014, 86, 7171−7183

of considerable importance (random coils, protein aggregates, etc.), but once such structures exceed 50 to 100 nm, their sizes are well-described by their particle-like nature without appeal to their molar mass. Although the particle molar mass may be of interest, in general, particle concentrations (following fractionation) are so low that their interactions may be neglected.

If we are to interpret the measurements of such carbon nanotubes as reported in the cited references using the R−G approximation, then we should visit again the strictures of eqs 1−3. Consider eq 1. The SWCNTs studied are basically just graphene tubes. The refractive index of various forms of graphite itself is reported[36−38] in the ranges of (1.46 to 2.72) + (0.01 to 1.46) i at 550 nm. At 633 nm, using interferometric picometrology, Wang and Nolte[39] obtained a value for graphene directly as 3.0 +1.4i. On this basis, in water, eq 1 yields $|m - 1| = |((3.0 + 1.4i)/1.33) - 1| = |1.256 + 1.053i| = (1.578 + 1.11)^{1/2} = 1.64$, a value well in excess of satisfying eq 1 and the applicability of the R−G approximation. Or is it?

Some of the measurements in the cited references use the R−G approximation and, for the case of SWCNTs, yield values, of which many are well-confirmed by electron microscopy, for a range of lengths up to a few hundred nanometers. Looking more closely, we note that the volumetric composition of such tubes includes a large fraction of water (or the fluids in which they are suspended). Because the incident wavelength is far larger than the tube diameter, we should judge the applicability of the R−G approximation based on the volume-weighted refractive index rather than the thin graphene container alone. Let us calculate this value.

The volume per unit length of a tube of radius a and thickness t is just $\pi t(2a - t)$. The diameters, however, are only about 1.2 nm, and the thickness of the graphene itself should be about the diameter of the carbon atom or 0.154 nm. Thus, the volume of the core water per unit length is about πa^2, where a = 0.6 − 0.154 = 0.446 nm, with the 0.154 nm value representing the radius of the carbon atom. Weighting πa^2 by the refractive index of water, about 1.33, and $\pi t(2a - t)$ by the refractive index of graphene (about 3 + 1.4i) and dividing by the unit volume πa^2, we obtain $|m - 1| \approx 0.73$. This is a huge value, certainly well beyond the strictures of even eq 3 except possibly for extremely small angles. This suggests immediately that if we are to have any chance of deriving physical properties from the measurements based on R−G theory, then application of eq 3 will be essential. Thus, measurements at small scattering angles might permit reasonably good estimates of the mean square radius $\langle r_g^2 \rangle$ from which the tube lengths may be derived from eq 24. Indeed, as we have confirmed already for relatively large polystyrene latex spheres (a = 500 nm) for which $|m - 1| \approx 0.2$, we might hope to obtain some reasonable results therefrom even for nanotubes of the types reported here. As the tube lengths reported in the cited references are in the tens of nanometers, terms involving a and t are negligible and may be dropped to determine L directly from the corresponding rms radius.

It is important to note that as long as structures have effectively weighted refractive indices that are close to those of the surrounding medium, as discussed herein, the results expected for sizes derived from mean-square radius values can be both useful and reasonably accurate (say, ±10%). However, if the effective refractive indices are too large, then the R−G approximation will fail. For example, if the SWCNTs were actually wires, e.g., the effective refractive index is that of graphene (large and complex), there is no chance for applicability. The stricture of eq 1, $|m-1| \ll 1$, is a major requirement of the R−G approximation, and, although a value of 0.2 is not as small as would be preferable, the additional restrictions of eq 3 will often result in the ability to deduce useful information. Recall the work of Mie,[18] who tried to explain the scattering of light from metallic particles. Despite the very small size of those particles of greatest interest for him (gold sols responsible for the remarkable colors seen following their illumination by light), use of the R−G approximation was never a consideration. Although not metallic, the structural constituents of SWCNTs make their light scattering characteristics deserving of far more detailed attention than simpler R−G describable scattering events.

In 2005, our laboratory examined a set of SWCNTs combining A4F and MALS for the first time to fractionate and then measure such particles. Particles were prepared following the procedures described in refs 40 and 41. In that short period of time during which our laboratory studied SWCNTs, we experienced considerable difficulties in obtaining and measuring such nanotubes of relatively restricted lengths. Some of these early results are shown in Figure 6. A slice (no. 757) is shown in Figure 7 as fit to the ill-fitting rod model of eq 19. The data do not fit the model. This rod model failure was seen also for some measurements reported by Gigault et al.[34] Although the rod model does not fit the data well (from Figure 7, the length based on the rod model is calculated as 214 ± 4 nm), this does not mean the nanotubes cannot be treated as very thin rods. It does suggest that eq 2 is not well satisfied.

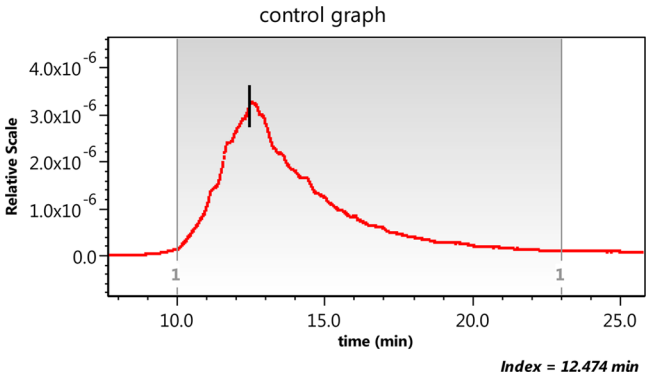

Figure 6. Elution profile of SWCNT sample. Slice 757 (elution time 12.474 min) is marked.

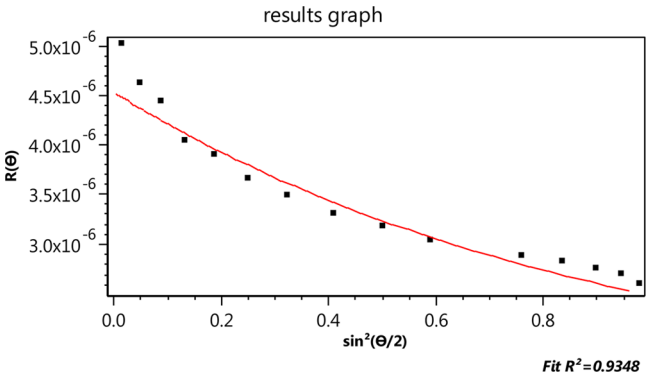

Figure 7. Fit of slice 757 of SWCNT data to the rod model.

dx.doi.org/10.1021/ac500185w | Anal. Chem. 2014, 86, 7171−7183

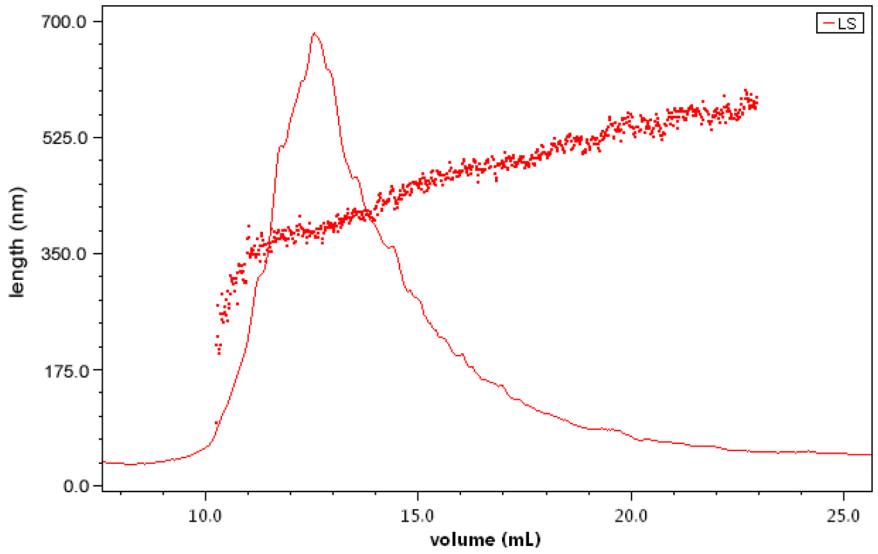

Figure 8. Nanotube length as a function of elution volume for SWCNT sample.

The nanotubes considered here (of length L and radius a) are well-characterized as very thin rods of length L because their diameters are negligible compared with their length ($a \ll L$). The reason the fit is so poor, however, arises from the fact that for every angles shown the condition of eq 3 is not satisfied. However, if we measure the slope of the angular variation in $\sin^2 \theta/2$ extrapolated to 0°, then we obtain an rms radius of 110.5 ± 13.2 nm, corresponding to the more probable length of 383 ± 46 nm. Taking the dimension $2a$ of eq 2 to correspond to the length L of a rod, we have $x = L/\lambda = (n_0 L)/\lambda_0 = (1.33x383)/(658) \approx 0.8$. Because $|m-1| \approx 0.73$, the requirement for a satisfactory application of the R−G approximation, i.e., just applying eq 19 and fitting, cannot be expected to suffice. The best we can hope for is the validity of eq 3 at very small angles with a relatively accurate measure of the mean-square radius, as shown.

Figure 8 presents the nanotube length as a function of elution volume based on calculation of its rms radii calculated from eq 24 with a and t both assumed to be $\ll L$. Note their very large sizes that explain, for example, why the rod model (per Figure 7, for example) is a poor interpretation of the measurements. Only the application of both eqs 3 and 16 at very small angles may be sufficient to obtain approximate sizes. The sizes (note the very small fractions present in the sample) below about 400 nm in Figure 8 might be accurate (±10%), but as the nanotubes become even larger, additional calculations at very small angles become necessary to yield comparable accuracies. Because the data are very old, we searched for records of microscopy measurements, but we found none. Such measurements might have confirmed explicitly the results of Figure 8. In the absence of explicit microscopy measurements, the deductions of Figure 8 cannot be considered reliable. What will be required, for future confirmation of the use of $\langle r_g^2 \rangle$ to derive size of such complex rods by MALS measurement, will be new measurements, such as those performed by the NIST and Gigault groups, supplemented by concurrent electron and/or AF microscopy.

MORE GENERAL SHAPES AND THE RMS RADIUS REVISITED

For many types of particles such as thicker rod-like particles, planks, ellipsoids, multiparticle aggregates such as shown in Figure 1 as well as those of even greater complexity, there are no simple structures easily associated with the recorded scattering data. Even a simple ellipsoid in the R−G approximation has to be averaged over all of its orientations, relative to the direction of the incident light, preparatory to deriving a best fit to the scattering data recorded from a suspension of such (required to be monodisperse) particles. Hopefully, from such a best fit, the dimensions of the suspended particles may be derived.

We have seen already, for the simple thin rods, that their lengths often may be derived from the measured rms radii. The rms radius, $\langle r_g^2 \rangle^{1/2}$, as defined simply by eq 12, is based entirely on the distribution of mass within a particle and does not depend upon any approximation. Its relation to the forward scattered intensity for any type of R−G particle, as long as eq 3 is valid, seems to be a reasonable basis for postulating that such initial slope measurements at $\theta = 0$ will produce a mean-square radius value from which quite accurate important dimensional information on the scattering particles may be derived. It is important to note, in the limit of measurements of light scattered at $\sin \theta/2 = 0$, that the scattered intensity is independent of the particle's orientation to the incident direction. Of course, if measurement is to be made from a suspension of particles, then such particles must be monodisperse, and the conditions of eq 3 must be satisfied.

We have seen from the rather simple polystyrene latex spheres discussed and studied in this perspective that the rms radii yield spherical radii with less than a 10% deviation from the exact Lorenz−Mie fits. It is interesting to reflect again on the work of Kerker[14] et al., whose motivation in studying the validity of the R−G theory was to explore the possibility of simplifying the calculations required to derive the structure of spherical particles of various refractive indices. Because the only parameters associated with the spheres that they studied were their refractive index and radius, only the radius might have been derived from the simpler R−G theory. The R−G approximation is not a function of the refractive index other

dx.doi.org/10.1021/ac500185w | Anal. Chem. 2014, 86, 7171−7183

than in a multiplicative factor as indicated, for example, in eq 4. Its key functional dependence on shape and structure is in the form factor $P(\theta)$, which is not dependent on the refractive index of the particle, always assumed to be almost the same as the surrounding medium per eq 1.

When combined with ancillary measurements, as might be obtained from electron or atomic force microscopy, the rms radius results could be expected to yield even more important physical structure information. A paper by Elazzouzi-Hafraoui et al.,[42] for example, discussing crystalline nanoparticles prepared from native cellulose, pointed out that some of the particles produced were in the form of planks (see eq 27) having length, width, and thickness. The Guan paper[30] also made reference to particles sharing similar properties. Consider, therefore, a sample of rods of the same radius a (thickness $2a$) and differing lengths L. Once fractionated by A4F, a distribution of lengths L_i based on the corresponding rms radius measured at each eluted fraction may be derived easily at each slice i from

$$L_i = \sqrt{12\langle r_g^2\rangle_i - 6a^2} \tag{34}$$

Reference 30 presents some excellent electron microscopy data showing the uniformity of fiber thickness for the samples measured. Referring to the cellulose rods of Figure 5 discussed above, consider the changes of the derived lengths if we include the thickness measurements of ref 30. In the particular sample, whose thicknesses were measured, the rods measured were cylindrical and of identical radii a = 5 nm. Table 3 shows, for three slices spanning the range of elution of Figure 5, how the application of eq 34 using such a relatively small 5 nm radius affects the actual rod lengths derived. The A4F separation of such rods is based on their effective hydrodynamic size, which is generally a function of both a and L. The possibility of extending the utility of the rms radius concept for the characterization of more complex particles, for which some structural elements are known *a priori*, is of considerable practical importance for measurements of nanoparticles. It is expected that the concepts discussed in this perspective will be used more frequently for the characterization of nanoparticles suitably fractionated and then measured by appropriate MALS instrumentation.

Table 3. Effect of Model and Rod Thickness on Derived Length

slice no.	length (rod model)	rms radius $\langle r_g^2\rangle^{1/2}$	length $(12)^{1/2}\langle r_g^2\rangle^{1/2}$	length per eq 34 for a = 5 nm
827	80	25 ± 2	87	74
1026	161	50 ± 2	173	169
1137	209	64 ± 1	222	221

SUMMARY

The term nanoparticles has been chosen to characterize particles with one dimension or feature less than 100 nm. A wide range of such particles, suspended in aqueous solutions, is well-characterized by the R−G approximation when applied suitably. Such application should be used only when the anticipated refractive index of the particles, the size-to-wavelength ratios, and the scattering angles selected/available are compatible with the strictures of eqs 1 and 3. If the particles are known *a priori* to be homogeneous spheres, then all angular scattering data available (weighted appropriately by the corresponding measurement standard deviations) should be used for fitting to the Lorenz−Mie theory. For all other cases, application of R−G approximation is best achieved by extracting the mean-square radii of the model chosen on the basis of all prior known or assumed particle structures. For all interpretations, based on Lorenz−Mie theory or the R−G approximation, particle samples must be fractionated before measurement to ensure that measurements are made from monodisperse samples. The accurate application (±10%) of the R−G approximation-derived rms radii to characterize homogeneous polystyrene latex spheres of sizes up to 1000 nm suggests that comparable particles of different shapes and relative refractive index ratios m, where $|m - 1| < 0.3$ (or perhaps even <1), might also be well-characterized through measurement of their rms radii. The jury is still out.

A final reminder on the use of the term particle. Treating such particles as molecules, and applying much of the molecular theory described well in the cited references, is fraught with inherent confusion or misinterpretation. Extracting molar masses of particles is neither appropriate nor applicable to understanding the structural elements characteristically associated with nanoparticle measurements.

AUTHOR INFORMATION

Corresponding Author

*E-mail: pwyatt@wyatt.com.

Notes

The author declares no competing financial interest.

ACKNOWLEDGMENTS

Dr. Wei Gao of Dow Chemical provided detailed data from her earlier detailed studies of polystyrene latex spheres spanning a broad range of sizes. The precision of these data provided much of the author's insights into the developments reported here. David Villalpando prepared the drawings and tables for this paper. Dr. Michelle Chen directed the steric A4F measurements of the SWCNT samples. Dr. Sigrid Kuebler is thanked for her measurements of cellulose nanofibers. Dr. Aym Berges made a variety of A4F fractionations and MALS measurements needed to confirm the applicability and limitations of the R−G approximation. He, together with Dr. David Rahmlow, tried (and often succeeded in) preparing SWCNT samples. They both made a variety of measurements on such and related samples, none of which are reported here. Dr. David Rahmlow also pointed out an error of the author in calculating some of the rms radii of sphere aggregates. Crystal Forsher performed much of the proofreading and reference organization of the paper. Richard Thomas prepared special graphing tools for using the ASTRA software that are now incorporated in the latest versions. Natalia Uruk assisted in the preparation of the final manuscript following the editorial and reviewers' requests for a far shorter presentation. That task proved to be far more challenging than expected, as she also discovered (and corrected) numerous errors and misprints in the perspective itself.

REFERENCES

(1) Jackson, C.; Nilsson, L.; Wyatt, P. J. *J. Appl. Polym. Sci.* **1989**, *43*, 99−114.
(2) Wyatt, P. J. *Anal. Chim. Acta* **1993**, *272*, 1−40.
(3) Wyatt, P. J. *High Polym.* **2011**, *60*, 816−820.
(4) Shortt, D. W. *J. Liq. Chromatogr.* **1993**, *16*, 3371−3391.

(5) Shortt, D. W. *J. Chromatogr. A* **1994**, *686*, 11−20.
(6) Van de Hulst, H. C. *Light Scattering by Small Particles*; John Wiley & Sons: New York, 1957.
(7) Wyatt, P. J. *Appl. Opt.* **1968**, *7*, 1879−1896.
(8) Debye, P. J. *Appl. Phys.* **1944**, *15*, 338−342.
(9) Debye, P. J. *J. Phys. Colloid Chem.* **1947**, *51*, 18−32.
(10) Chanda, M. *Introduction to Polymer Science and Chemistry: A Problem Solving Approach*; CRC Press: Boca Raton, FL, 2006.
(11) Kratochvil, P. *Classical Light Scattering from Polymer Solutions*; Elsevier: Amsterdam, The Netherlands, 1987.
(12) Zimm, B. H. *J. Phys. Chem.* **1948**, *16*, 1093−1099.
(13) Kerker, M. *The Scattering of Light and Other Electromagnetic Radiation*; Academic Press: New York, 1969.
(14) Kerker, M.; Farone, W. A.; Matijevic, E. *Appl. Opt.* **1963**, *53*, 758−759.
(15) Lorenz, L. V. *Vidensk. Selsk. Skr.* **1890**, *6*, 1−62.
(16) Logan, N. A. *Proc. IEEE* **1965**, *53*, 773−785.
(17) Wyatt, P. J. *Appl. Opt.* **1974**, *13*, 2751.
(18) Mie, G. *Ann. Phys.* **1908**, *25*, 377−442.
(19) Zimm, B. H. *J. Phys. Chem.* **1948**, *16*, 1099−1116.
(20) Wyatt, P. J. *Nature* **1970**, *226*, 277−279.
(21) Quist, G. M.; Wyatt, P. J. *J. Opt. Soc. Am. A* **1985**, *2*, 1979−1986.
(22) Kattawar, G. W.; Dean, C. E. *Opt. Lett.* **1983**, *8*, 48−50.
(23) Striegel, A.; Yau, W. W.; Kirkland, J. J.; Bly, D. D. *Modern Size-Exclusion Liquid Chromatography: Practice of Gel Permeation and Gel Filtration Chromatography*, 2nd ed.; John Wiley & Sons, Inc.: Hoboken, NJ, 2009.
(24) Podzimek, S. *Light Scattering, Size Exclusion Chromatography, and Asymmetric Flow Field Flow Fractionation: Powerful Tools for the Characterization of Polymers, Proteins and Nanoparticles*; John Wiley & Sons, Inc.: Hoboken, NJ, 2011.
(25) Wyatt, P. J. *J. Colloid Interface Sci.* **1998**, *197*, 9−20.
(26) Wyatt, P. J.; Weida, M. J. U.S. Patent 6,774,994, 2004.
(27) Kuebler, S. Unpublished work.
(28) Wyatt, P. J.; Villalpando, D. N. *Langmuir* **1997**, *13*, 3913−1914.
(29) Refractive Index Database. refractiveindex.info/.
(30) Guan, G.; Cueto, R.; Russo, P.; Qi, Y.; Wu, Q. *Biomacromolecules* **2012**, *13*, 2671−2679.
(31) Ando, Y. *J. Nanosci. Nanotechnol.* **2010**, *10*, 3726−3738.
(32) Fagan, J. A.; Bauer, B. J.; Hobbie, E. K.; Becker, M. L.; Hight-Walker, A. R.; Simpson, J. R.; Chun, J.; Obrzut, J.; Bajpai, V.; Phelan, F. R.; Simien, D.; Huh, J. Y.; Migler, K. B. *Adv. Mater.* **2010**, *20*, 1−11.
(33) Chun, J.; Fagan, J. A.; Hobbie, E. K.; Bauer, B. J. *Anal. Chem.* **2008**, *80*, 2514−2523.
(34) Gigault, J.; Grassl, B.; Le Hécho, I.; Lespes, G. *Microchim Acta* **2011**, *175*, 265−271.
(35) Gigault, J.; Le Hécho, I.; Dubascoux, S.; Potin-Gautier, M.; Lespes, G. *J. Chromatogr. A* **2010**, *1217*, 7891−7897.
(36) Bond, T. C.; Bergstrom, R. *Aerosol. Sci. Technol.* **2006**, *40*, 27−67.
(37) Bond, T. C.; Anderson, T. L.; Campbell, D. *Aerosol. Sci. Technol.* **1999**, *30*, 582−600.
(38) Duley, W. W. *Astrophys. J.* **1984**, *287*, 694−696.
(39) Wang, X.; Nolte, D. *Complex refractive index of graphene measured by picometrology*, 2009 APS March Meeting, Pittsburgh, PA, March 16−20, 2009; http://meetings.aps.org/link/BAPS.2009.MAR.A25.12.
(40) Zheng, M.; Jagota, A.; Semke, E. D.; Diner, B. A.; McLean, R. S.; Lustig, S. R.; Richardson, R. E.; Tassi, N. G. *Nat. Mater.* **2003**, 338−341.
(41) Fagan, J. A.; Landi, B. J.; Mandelbaum, I.; Simpson, J. R.; Bajpai, V.; Bauer, B. J.; Migler, K.; Hight Walker, A. R.; Raffaelle, R.; Hobbie, E. K. *J. Phys. Chem. B* **2006**, *110*, 23801−23805.
(42) Elazzouzi-Hafraoui, S.; Nishiyama, Y.; Putaux, G. L.; Heux, L. *Biomacromolecules* **2008**, *9*, 57−65.